JGR Atmospheres

RESEARCH ARTICLE
10.1029/2020JD034000

Time Evolution and Diurnal Variability of the Parametric Sensitivity of Turbine-Height Winds in the MYNN-EDMF Parameterization

L. K. Berg[1], Y. Liu[1], Ben Yang[2], Y. Qian[1], R. Krishnamurthy[1], L. Sheridan[1], and J. Olson[3]

[1]Pacific Northwest National Laboratory, Richland, WA, USA, [2]CMA-NJU Joint Laboratory for Climate Prediction Studies and School of Atmospheric Sciences, Nanjing University, Nanjing, China, [3]NOAA-Global Systems Laboratory, Boulder, CO, USA

Key Points:

- Sensitivity to new parameters in the MYNN-EDMF parameterization is generally small, with the largest impact during daytime
- Parameter sensitivity is stable over the simulation period for both summer and winter
- There is a strong diurnal cycle in parameter sensitivity during the summer associated with atmospheric stability

Correspondence to:

L. K. Berg,
larry.berg@pnnl.gov

Citation:

Berg, L. K., Liu, Y., Yang, B., Qian, Y., Krishnamurthy, R., Sheridan, L., & Olson, J. (2021). Time evolution and diurnal variability of the parametric sensitivity of turbine-height winds in the MYNN-EDMF parameterization. *Journal of Geophysical Research: Atmospheres*, *126*, e2020JD034000. https://doi.org/10.1029/2020JD034000

Received 29 SEP 2020
Accepted 28 APR 2021

Author Contributions:

Conceptualization: L. K. Berg, Y. Qian
Data curation: Y. Liu, Ben Yang, R. Krishnamurthy, L. Sheridan
Formal analysis: L. K. Berg, Y. Liu, Ben Yang, R. Krishnamurthy, L. Sheridan, J. Olson
Funding acquisition: L. K. Berg
Investigation: Y. Liu, J. Olson
Methodology: L. K. Berg, Ben Yang, Y. Qian, J. Olson
Project Administration: L. K. Berg
Software: Y. Liu, Ben Yang
Supervision: L. K. Berg, Y. Qian
Validation: Ben Yang
Visualization: Y. Liu, Ben Yang
Writing – original draft: L. K. Berg
Writing – review & editing: L. K. Berg, Y. Liu, Ben Yang, Y. Qian, R. Krishnamurthy, L. Sheridan, J. Olson

Abstract The Mellor-Yamada-Nakanishi-Niino (MYNN) parameterization applied in the Weather Research and Forecasting (WRF) model has been augmented to include the Eddy-Diffusion Mass-Flux (EDMF) approach to better represent transport by boundary-layer eddies. This change includes the addition of new parameters associated with convective updrafts and boundary-layer clouds that lead to new parametric sensitivities in the turbine-height wind speed compared to simulations using the standard MYNN parameterization. This work builds on efforts focused on WRF's MYNN parameterization by examining the sensitivity of wind speed to parameters in the MYNN-EDMF parameterization as a function of simulation duration. Summer and winter periods were selected from the second Wind Forecast Improvement Project (WFIP2). Five sets of simulations were completed for each season, with durations ranging from 2 to 6 days. The results show that the sensitivity to the new parameters associated with the EDMF scheme is generally small compared to other parameters in clear conditions, but the sensitivity to the entrainment becomes significant when the updraft fraction is large. The spread in the perturbed parameter ensembles was found to grow quickly over the first 8–19 h in the summer simulations and 17–24 h in the winter simulations with little change after that, regardless of the simulation length. A strong diurnal cycle in the parameter sensitivity was also found associated with the atmospheric stability, as well as an increase in the sensitivity to the entrainment parameter used in the EDMF parameterization that is associated with increasing fractional area covered by plumes.

Plain Language Summary Atmospheric models, such as the WRF model, use mathematical representations to account for turbulence near the surface. These treatments are constantly evolving and have recently been modified to combine two different approaches, one part focused on small scale eddies and a second part to treat large eddies that span much of the planetary boundary layer. This treatment involves a number of parameters whose values are highly uncertain. The goal of this study is to examine the impact of parameter uncertainty on the simulated turbine-height wind speed for two periods, summer and winter, from a recent field study. In addition, the study was designed to test the parametric sensitivity of the turbine-height wind speed to simulation duration. We show that parameters associated with the treatment of large eddies are generally small compared to the other parameters, but becomes significant in daytime cases. The spread of the simulation ensemble grows quickly in the first 19–24 h of the simulation, but changes little after that, regardless of the duration. The analysis also investigates how the parametric sensitivity changes between stable and unstable conditions as different treatments are used in the parameterization for different stabilities.

1. Introduction and Motivation

Understanding the sensitivity of simulations to parameter values is an important step in determining the uncertainty in simulations using numerical models, such as the Weather Research and Forecasting (WRF) model (Skamarock et al., 2008). The uncertainty introduced by the boundary-layer parameterization is particularly important for wind energy applications and has been the topic of a series of studies focused on the Pacific Northwest of the United States (Berg et al., 2019; Yang, Berg, et al., 2019; Yang, Qian, et al., 2017). The work of Yang et al. (2017) delved into the parametric sensitivity of the Mellor-Yamada-Nakanishi-Niino

(MYNN) (Nakanish, 2001; Nakanishi & Niino, 2004, 2006, 2009) and found that much of the spread in an ensemble of simulations can be attributed to a relatively small number of parameters in their summer case study. This work was augmented by Berg et al. (2019) to include analysis of both summer and winter conditions over the same region. Yang et al. (2019) extended the work further to include both the Yonsei University and MYNN parameterizations in a study of both parametric and structural uncertainty in WRF simulations. Other studies (e.g., Banks et al., 2016; Carvalho et al., 2012; Constantinescu et al., 2011; Fernández-González et al., 2018; Smith & Ancell, 2019) have also examined structural uncertainty associated with the parameterizations used in WRF or the impact of uncertainty in initial and boundary conditions of WRF for wind energy applications.

Recently, the MYNN parameterization has been augmented to include Eddy-Diffusion Mass-Flux (EDMF) in the WRF model (Olson, Kenyon, Angevine, et al., 2019) to better represent vertical transport associated with large boundary layer eddies. This implementation includes multiple subgrid plumes, with the number of plumes determined dynamically based on surface and boundary layer properties. Subgrid cloud fraction in this implementation is based on the subgrid cloud probability density function following Sommeria and Deardorff (1977). The EDMF approach was designed to improve the representation of local and non-local transport in both clear and cloudy boundary layers (e.g., Angevine, 2005; Angevine et al., 2010; Neggers, 2009; Neggers et al., 2009; Siebesma et al., 2007; Soares et al., 2004; Sušelj et al., 2012; Tan et al., 2018). In their analysis of results from the NOAA High-Resolution Rapid Refresh (HRRR) model, Olson, Kenyon, Djalalova, et al. (2019) found significant improvements in the forecast of turbine-height wind speed using the MYNN-EDMF parameterization (among other model changes) compared to the default MYNN parameterization for tests during the second Wind Forecast Improvement Project (WFIP2).

Other studies have examined the parametric sensitivity in the EDMF parameterization outside of the WRF implementation used here. Suselj et al. (2020) examined the sensitivity of the Jet Propulsion Laboratory version of the EDMF parameterization and found strong sensitivity to the entrainment in the mass-flux part of the parameterization for case studies with boundary layer clouds. Langhans et al. (2019) also looked at the parametric sensitivity of the EDMF parameterization in a single column model and found sensitivity to the plume entrainment and the initial plume properties.

In this study, we build on earlier work to extend the sensitivity study to include the new MYNN-EDMF parameterization. We investigate how the sensitivity changes as a function of simulation duration and we focus on the time evolution of the turbine-height wind speed rather than monthly means. While a large number of studies have examined the sensitivity of model results with forecast lead time (e.g., Ancell, 2016; Etherton & Santos, 2008; Fernández-González et al., 2017), only a small number of studies have examined the parametric uncertainty as a function of forecast lead time. Di et al. (2015) found that, in general, the parameters that explain the variability of convective storms were independent of forecast lead time. In contrast, Xu et al. (2020) found some sensitivity to lead time for variables above 850 mb, but there was less sensitivity close to the surface.

The manuscript is arranged as follows. The second section provides a description of the WRF model as used in this study, describes the experimental configuration and the parameters that were selected, and briefly describes the sensitivity analysis approach. The third section provides a brief description of WFIP2 data sets used to evaluate model performance for the summer and winter cases. The fourth section presents the results as a function of simulation period and time of day.

2. Model Configuration, Parameter Selection, and Sensitivity Analysis Approach

The Advanced Research WRF model version 3.9 is used (Skamarock et al., 2008) in this study. The single model domain covers the northwestern United States and includes the WFIP2 study domain (Figure 1). The model domain is configured with horizontal grid spacing of 3 km and has 380 and 350 grid points in the east-west and north-south directions, respectively, and 55 vertical layers. The vertical grid spacing is approximately 15 m within 200 m of the surface and 10 to 28 model layers are generally found in the planetary boundary layer (PBL).

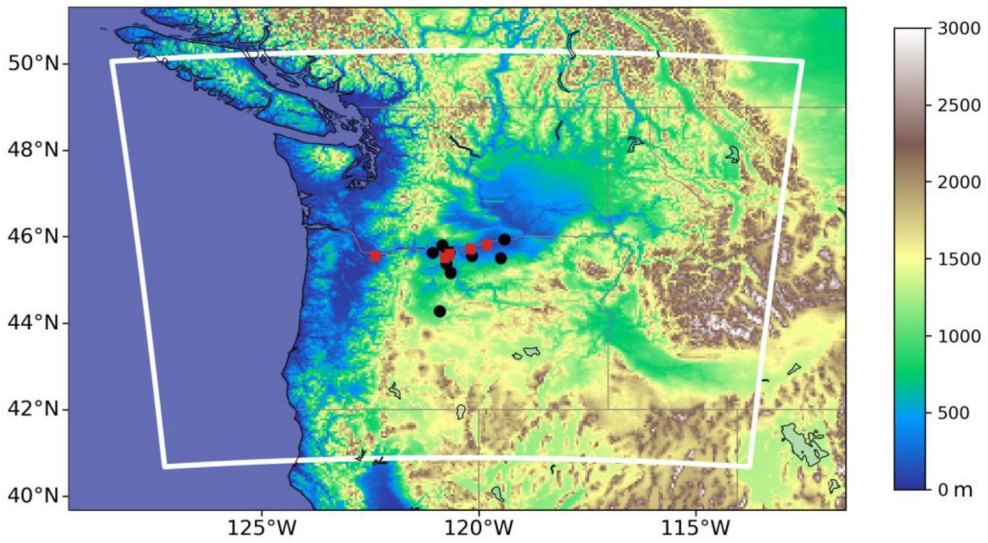

Figure 1. Model domain (white) with terrain elevation indicated by colors. Symbols indicate WFIP2 sodar (black circle) and lidar (red squares) locations.

A standard set of model physics is used in all simulations shown in this study. The PBL and shallow convective processes are represented by the MYNN-EDMF PBL scheme (Nakanishi & Niino, 2006, 2009; Olson, Kenyon, Angevine, et al., 2019). Other model physics include the MYNN surface layer scheme (Dyer & Hicks, 1970), Rapid Radiative Transfer Model (Iacono et al., 2008) long-wave and short-wave radiation schemes, and the aerosol-aware Thompson microphysics scheme (Thompson & Eidhammer, 2014; Thompson et al., 2008). The Rapid Update Cycle land surface model (Smirnova, Brown, & Benjamin, 1997; Smirnova, Brown, Benjamin, & Kenyon, 2016; Smirnova, Brown, Benjamin, & Kim, 2000) is used to represent surface processes. Boundary and initial conditions are from the North American Regional Reanalysis (Mesinger et al., 2006).

This particular study was designed to investigate the sensitivity to 11 parameters as a function of simulation duration for two periods selected from WFIP2, one in summer and one in winter. Perturbed parameters ensembles (PPEs), each with 128 members, were generated using the quasi-Monte Carlo sampling approach (Caflisch, 1998) for simulations with durations ranging from two to six days with a common end date for each season; August 24, 2016, and January 17, 2017. The application of this technique is to achieve better dispersion of the parameter selections compared to random or pseudorandom approaches. The selection of different seasons is designed to allow for the examination of the parameter sensitivity in both unstable and stable conditions.

Previous studies (Berg et al., 2019; Yang, Qian, et al., 2017) focused on the sensitivity of simulated turbine-height (taken to be 80 m above the surface) wind speed to parameter values used in the standard MYNN parameterization. They found the greatest sensitivity to Turbulence Kinetic Energy (TKE) dissipation rate (B_1), turbulent Prandtl number (Pr), factors associated with turbulence length scales applied within the MYNN parameterization (α_1, α_4, α_5, and β), surface roughness (represented by the scaling factor, $Z_{F,}$ that is applied to the standard representation of surface roughness), and the von Karman constant (K). These parameters are carried into the present study, but three additional parameters associated with the EDMF parameterization are also included. These new parameters, c_σ, α_{conv}, and c_ε, are associated with the properties of convective plumes and the treatment of boundary layer cloud fraction within the model grid cell. Other parameters could be tested as well, but this subset is consistent with the results of Suselj et al. (2020), who found strong sensitivity to the entrainment. Values for the various parameters were based on values that have appeared in the literature, or in cases where additional information is not available increased or decreased by approximately a factor of two, and are listed in Table 1.

Table 1
Parameter Names, Physical Meaning, Default Value and Range Applied in This Study

Parameter	Physical Meaning	Default Value	Range
B_1	Applied in TKE dissipation rate	24	18-30
Pr	Prandtl Number	0.74	0.5-2
α_1	Parameter in turbulence length scale	0.23	0.16-3.0
α_4	Parameter in turbulence length scale	20	0-100
α_5	Parameter in turbulence length scale	2.1	1.35-4.05
β	Parameter in turbulence length scale	0.2	0.1-0.3
Z_F	Scaling factor for surface roughness	1	1.0-2.0
K	Von Karman constant	0.4	0.35-0.40
c_σ	Scaling factor for contribution to standard deviation of saturation deficit (s) due to stratus	0.225	0.2-0.25
α_{conv}	Scaling factor for contribution to standard deviation of s due to mass flux	$6.0\text{x}10^{-3}$	$3.0\text{x}10^{-3}$-$12.0\text{x}10^{-3}$
c_ε	Scaling factor for entrainment	0.5	0.3-0.9

Note. Shaded areas indicate parameters associated with the EMDF representation.

Within the MYNN-EMDF parameterization implemented in WRF (Olson, Kenyon, Angevine, et al., 2019) the entrainment in individual plumes is defined as a function that is inversely proportional to the updraft speed and the plume size (Tian & Kuang, 2016):

$$\varepsilon_i = \frac{c_\varepsilon}{w_i d_i}, \tag{1}$$

where w and d are the updraft speed and plume diameter, respectively and i indicates the specific updraft. Tian and Kuang (2016) suggested a value of 0.46 m s^{-1}, but they note that this value is determined empirically and may vary with the TKE and is set to 0.5 or 0.35 depending on the version of the WRF model. In this study, it is allowed to range between 0.3 and 0.9. The cloud fraction in the parameterization is defined in terms of the distribution of the saturation deficit (s) as described by Chaboureau and Bechtold (2002, 2005) and Olson, Kenyon, Angevine, et al. (2019). The variability of s for stratus is defined as:

$$\sigma_{s-strat} = c_\sigma l \left[a^2 \frac{\partial q_t}{\partial z} - \frac{2ab}{c_{pm}} \frac{\partial h_l}{\partial z} \frac{\partial q_t}{\partial z} + \frac{b^2}{c_{pm}^2} \left(\frac{\partial h_l}{\partial z} \right)^2 \right]^{1/2}, \tag{2}$$

where a and b are thermodynamic functions, l is the mixing length determined in the turbulence parameterization, h_l is the grid-box moist static energy, q_t is the total water mixing ratio, z is the height, c_{pm} is the specific heat capacity of moist air, and c_σ is a constant. The default value of c_σ applied in WRF is 0.225, while a value of 0.2 was suggested by Chaboureau and Bechtold (2002) and its value is allowed to range over 0.2 to 0.25 here. The expression for the variability of s for convective clouds is defined in terms of the cloud mass flux, M, and a vertical scaling function taken to be α^{-1}:

$$\sigma_{s-conv} \approx \alpha_{conv} M a^{-1}, \tag{3}$$

where α_{conv} is a proportionality constant that was originally assumed to be 5×10^{-3}, but is allowed to range between 3×10^{-3} and 12×10^{-3} in this study. The values of the variability of the saturation deficits are combined to estimate the cloud fractional area, as described by Olson, Kenyon, Angevine, et al. (2019).

3. Data Sets and Weather Conditions

Data used in this study include lidar and sodar observations collected during WFIP2 (Shaw et al., 2019) and details of the field deployment can be found in Wilczak et al. (2019). A number of different sodar makes and models were used, including Scintec MFAS and SFAS, Triton Wind Profiler, Atmospheric Sciences Corporation MiniSodar, and custom built sodars deployed by Argonne National Laboratory. The maximum

range of sodars varied between approximately 200 and 400 m, depending on the sodar type and atmospheric conditions. In addition, the overall quality of the sodar data was much better in summer than during winter. Lidar data were collected using several different systems, including: WindCube V1 and V2 profilers, WindCube 200s, ZephIR Profiler. In contrast to the sodars, the quality of the lidar data was generally independent of season (Pichugina, Banta, Bonin, et al., 2019). In this analysis, hourly domain averages and standard deviations of turbine-height wind speed (assumed to be 80 m above the surface) were computed using all good data from the sodars and lidars at that given hour. In total data from 9 sodars and 6 lidars were used to compute the summertime values, and data from 4 sodars and 4 lidars were used to compute the wintertime values. There was generally good agreement between the measurements from the two different systems (not shown).

A detailed event log was developed during WFIP2 that includes descriptions of weather events and classifies the meteorological conditions on given days based on the analysis of scientists working on the project team (https://a2e.energy.gov/data/wfip2/log.z01.00). Two periods were selected for this study to cover a range of different stabilities as well as relatively strong and weak winds. The summer period (August 18 through 24, 2016) was marked with cross barrier winds over the Cascade Range driven by synoptic scale flow and thermal differences between the coast and the Columbia Basin (Banta et al., 2020). This period includes days with domain average turbine-height wind speeds ranging from approximately 2 to 14 m s^{-1} (Figure 2). The winter period (January 11 through 17, 2017) was marked by a frontal passage at the start of the period and the presence of cold pools during which cold air was trapped in the basin, periods with easterly flow, and generally weaker domain averaged winds that were less than 6 m s^{-1} for much of the simulation period (Figure 2), as highlighted by McCaffrey et al. (2019), Bianco et al. (2019), and Pichugina et al. (2020). The diurnal cycle was significantly muted during the winter period, which is typical for cold pool cases.

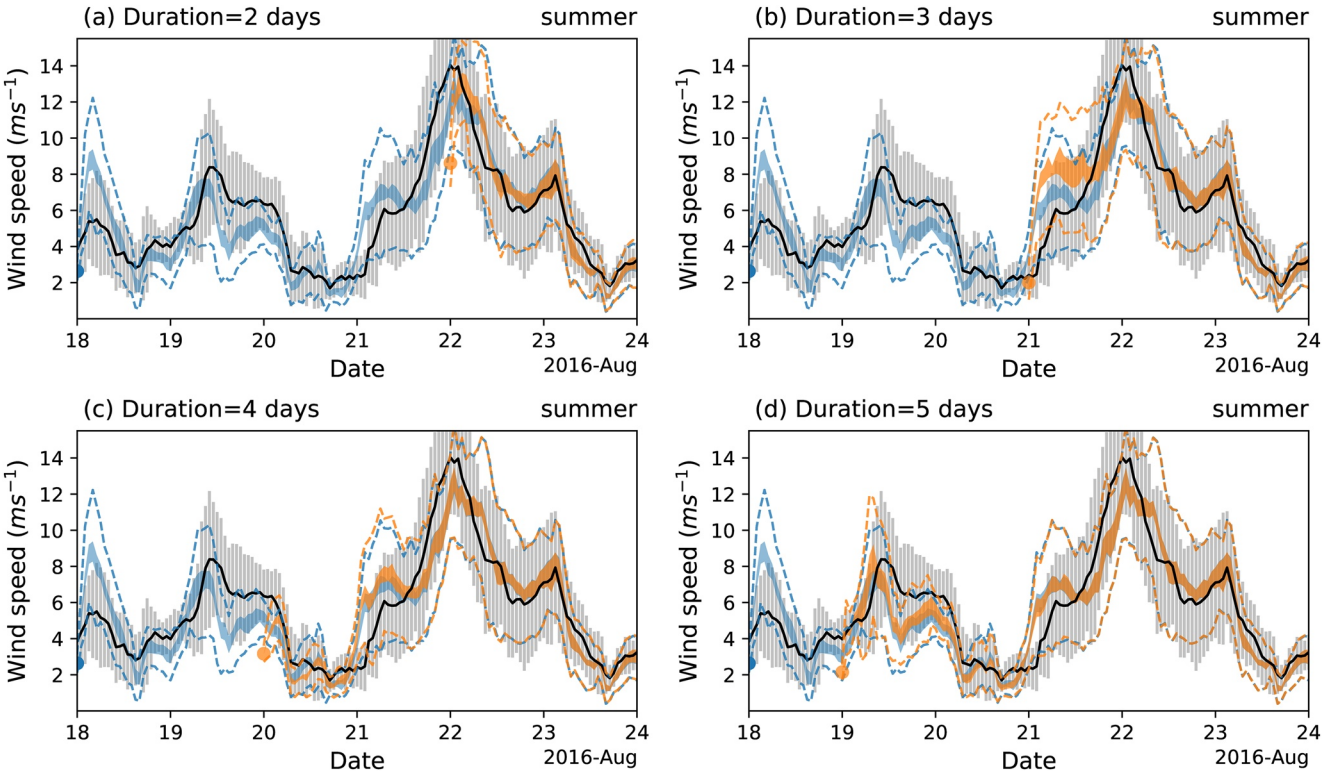

Figure 2. Time series of observed mean (black line) and standard deviation (gray shading) of turbine-height wind speed computed across sodar and lidar locations as well as time series of the simulated range between the 2.5 and 97.5 percentile of PPE member means (blue and orange shading—the mean over the entire PPE falls in the center of the shaded area) and standard deviation of the PPE mean (dashed lines) at the points in the domain with valid sodar or lidar measurements for various simulation durations in summer. Blue indicates the simulation conducted over the entire six-day period, and orange indicates shorter simulations with the orange dot indicating the start of the simulation period for cases with 2-, 3-, 4-, and 5-days duration.

4. Results

4.1. Comparison of Model Results With WFIP2 Data

The overall performance of the PPEs can be evaluated using observations from the sodars and lidars deployed during WFIP2. During the summer (Figure 2) there is generally good agreement between the average observed turbine-height wind speed and the range of simulated values (averaged over WRF grid points closest to the observation sites) from the PPE means. The magnitude, but not the timing, of the wind ramp event on August 19 is well captured, but the wind speed increase in the simulations from August 21 through 22 is smaller and is simulated to occur later than observed. The overall good agreement in wind speed when averaged across the measurement locations is likely due to the capture of the key synoptic scale features in the reanalysis data used to drive the simulations and the high quality of data from the sodars and lidars during the summer. The inter-member spread of the mean wind speed across all sites is generally quite small, as indicated by the blue shading for the simulation with 6 days duration and orange shading for simulations with 2, 3, 4, and 5 days duration in Figure 2, which represents the spread between the 2.5 and 97.5 percentiles of the PPE members. The standard deviation across all sites from the PPE mean is generally similar to the standard deviation of the observations (Figure 2). The good agreement between the standard deviations indicates that the simulation ensemble is able to capture the variability seen across the measurement locations.

The agreement between the simulated and observed turbine-height wind speed in the winter is better in the first half of the analysis period (through approximately January 14, Figure 3). Through January 12 the variability in the PPE means is almost as large as the observed standard deviation. Later in the period, however, the variance of the PPE increases, while the range of the PPE means is much smaller. The large values of wind speed on January 11 are associated with the passage of a cold front, as described in the WFIP2 event log. After the frontal passage, a cold pool set up over the Columbia Basin. During the cold pool, near-surface wind speeds were generally weak and the simulated wind speed was greater than observed. This behavior could be related to issues with the reanalysis, including initialization of the cold pools as well as the

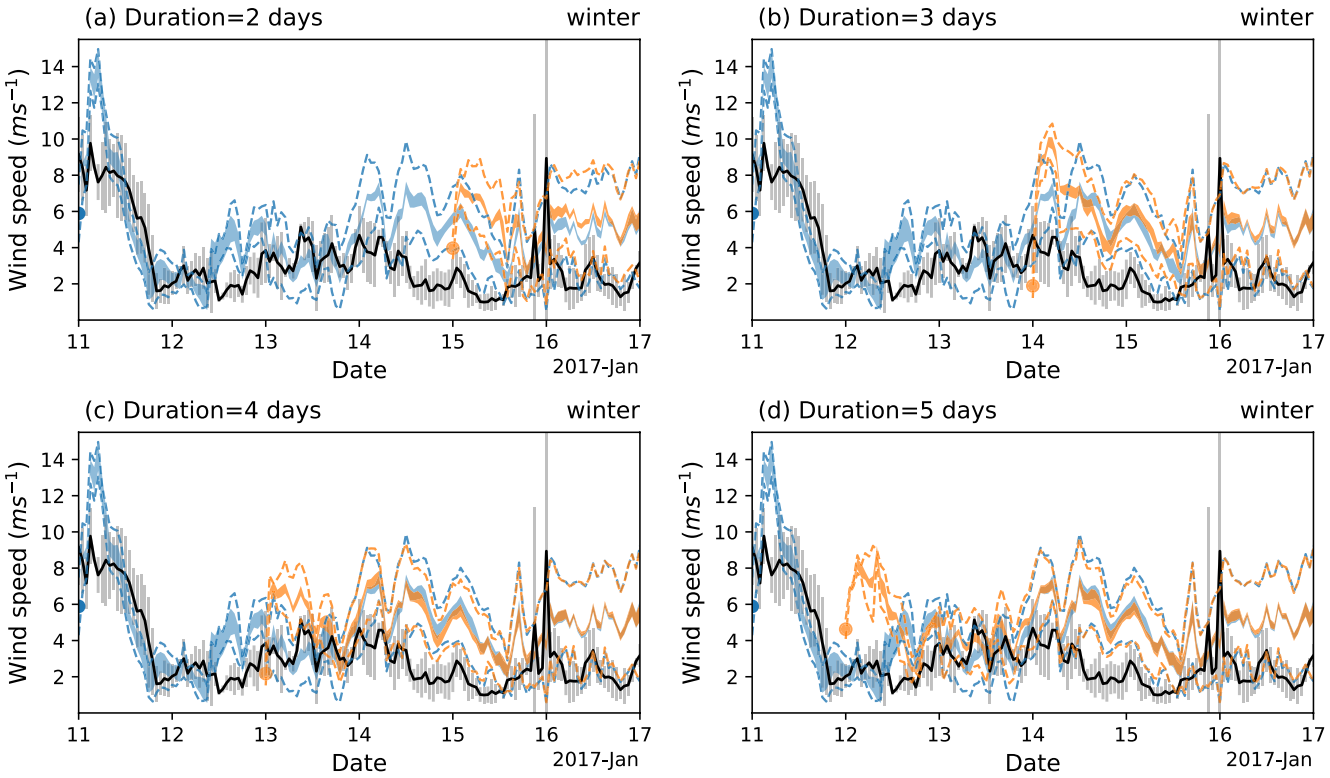

Figure 3. Same as Figure 2 but for the winter case.

well-documented issues associated with simulating cold pool evolution and/or the cold pool depth (e.g., Olson, Kenyon, Djalalova, et al., 2019; Pichugina, Banta, Bonin, et al., 2019; Pichugina, Banta, Alan Brewer, et al., 2020; Wilson & Fovell, 2016; Zhong et al., 2001). It is clear from these results that improvement in the representation of cold-pool dynamics is not possible by changing the parameter values used in the MYNN-EDMF parameterization, which is consistent with the results of Lu and Zhong (2014). There were also many more instances of poor data quality during the wintertime, which could contribute to the poorer agreement between the observations and the simulations.

4.2. Comparison of PPE Simulations With Previous Studies

Previous studies (Berg et al., 2019; Yang, Berg, et al., 2019; Yang, Qian, et al., 2017) focused on the sensitivity of simulated turbine-height wind speed to parameter values used in the standard MYNN parameterization. They found the greatest sensitivity to TKE dissipation rate, turbulent Prandtl number, turbulence length scales, surface roughness, and the von Karman constant. As described in Section 3, three additional parameters associated with the EDMF treatment have been added in this study. The generalized linear model (McCullagh & Nelder, 1989) was adopted to decompose the total variances from the 128 PPEs members completed with varying parameters into the contributions from each parameter as well as their interactions. The target variable V (i.e., wind speed here) is written as a function of input parameters in a fitting equation,

$$V = \beta_0 + \sum_{j=1}^{n} \beta_j * P_j + \sum_{j=1}^{n} \sum_{k=1}^{n} \beta_{j,k} * P_j * P_k + \varepsilon, \varepsilon \sim N\left(0, \sigma^2\right), \tag{4}$$

where $P_j \left(j = 1, \ldots, n\right)$ are input parameters; n is the number of parameters; β_0 represents the intercept coefficient; β_j and $\beta_{j,k}$ are the coefficients of linear and interaction terms; ε is the residual, which is assumed to follow an independent normal distribution and have zero mean. In this study, quadratic terms ($j = k$, i.e., P_j^2) are also included in the generalized linear model. The generalized linear model can be used in situations where either a linear or nonlinear model is valid and requires a single set of PPE simulations perturbing all parameters simultaneously, which reduces the number of simulations compared to approaches that perturb one parameter at a time and allows for the study of interactions among parameters. Other studies, such as those of Nielsen-Gammon et al. (2010) and Shi et al. (2014), used a combination of single-parameter and multiparameter approaches to determine the impact of individual parameters relative to the others and how large an impact the selection of parameters might have. The successful application of their approaches depends on the linearity between the parameters and model output (Shi et al., 2014). Besides, contributions of parameter interactions were not considered in their studies. The WRF model has a high degree of complexity and strong nonlinearities, therefore, the generalized linear model is applied in this study.

The generalized linear model builds a fitting equation and calculates the determination coefficient (R^2) of model fitness, as well as the statistical significance of the estimated coefficient and interpreted variance associated with each term in the fitting equation. The reduction in the sum of the square of residual caused by sequentially introducing each term, including linear, higher order, and interaction terms, is used to compute the relative contribution of individual parameters and their interactions.

The total variance of the WRF output (i.e., the turbine-height wind speed) into the contribution from different parameters on August 22 for the simulation with 2 days duration is shown in Figure 4. In general, the results show greater sensitivities to the parameters associated with the standard MYNN parameterization than the parameters added for the EDMF representation (c_σ, α_{conv}, and c_ε). The relatively small impact associated with for c_σ and α_{conv}, is not surprising as they are only active in cloudy conditions, and boundary layer clouds were infrequent during the study periods. There is sensitivity to c_ε, during the daytime when the mass-flux component of the EDMF parameterization is active and its sensitivity is largest in a fully developed convective boundary layer when the EDMF plumes are active. This behavior will be revisited again and explored in more detail in Section 4.4 looking at the diurnal evolution. When nighttime conditions are considered the values of Pr, α_1, α_5, Z_F and K have the largest impact on the wind speed, which is consistent with previous results of Yang et al. (2017) and Berg et al. (2019) (not shown) and are very similar to the winter results described next.

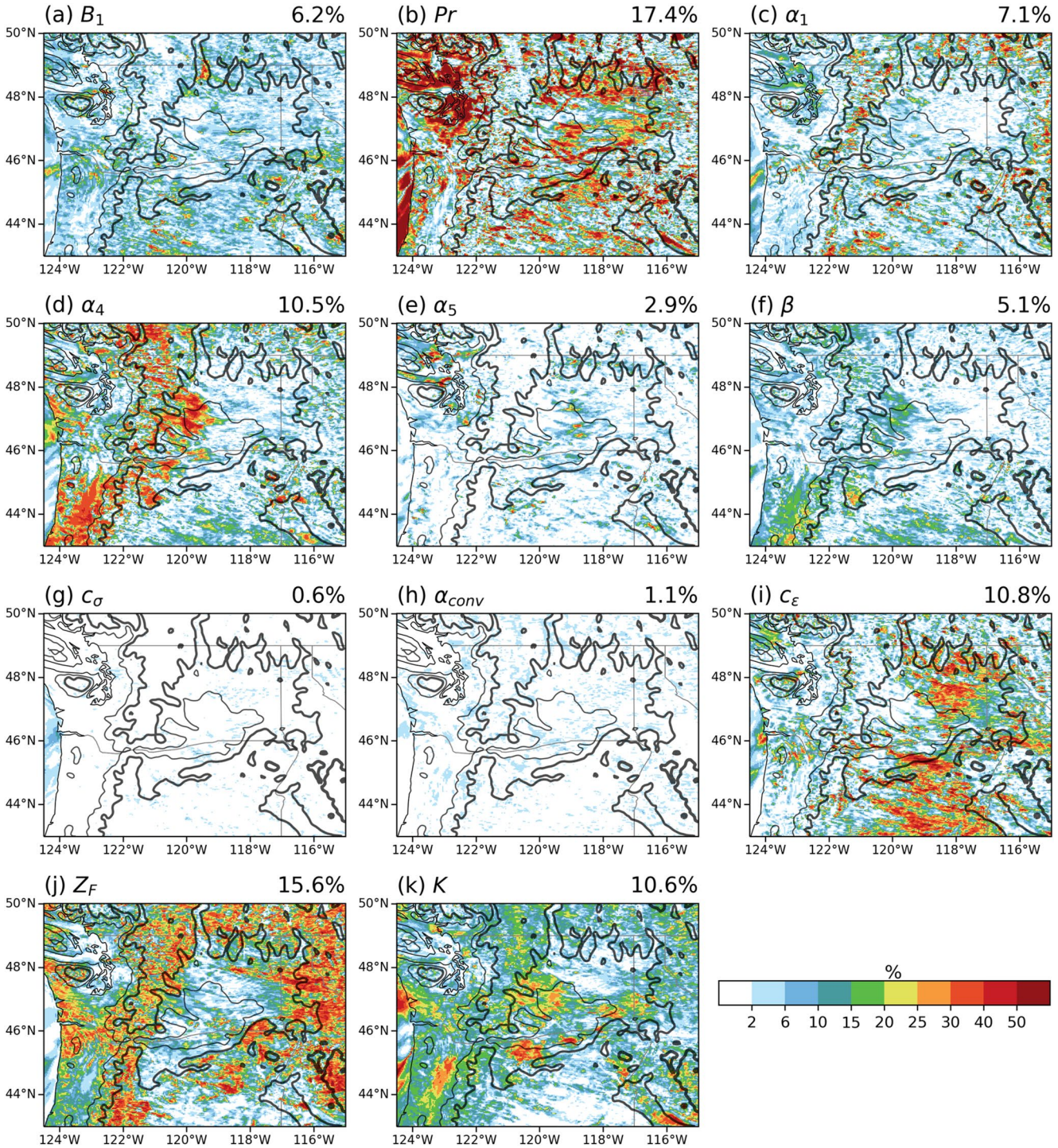

Figure 4. Fraction of the variance of turbine-height wind speed explained by each parameter in Table 1 for August 22, 2016 (simulation of 2 days duration) during daytime. Lines indicate terrain elevations of 500 (thin) and 1,000 m (thick). Numbers on the top-right corner of each panel indicate the variance explained by each parameter.

During the winter case study, the meteorological conditions at the start of the study period were marked by the frontal passage and associated cloud cover. After the frontal passage on January 11, conditions were dominated by persistent cold pools, clear skies, and generally weak winds (Figure 3) consistent with stable conditions. Results from the daytime on January 15 for the simulation of 2 days duration (Figure 5), are

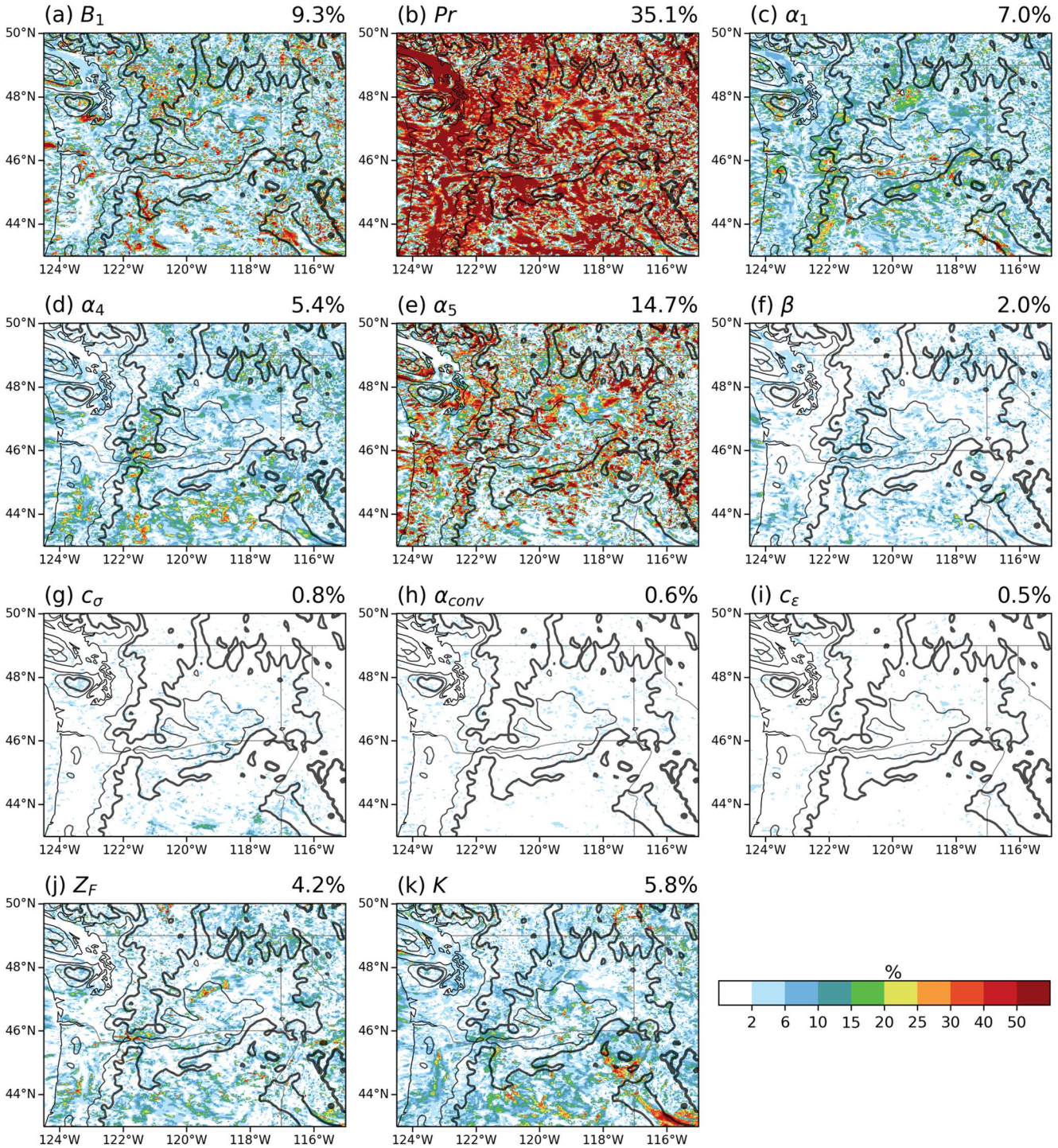

Figure 5. Same as Figure 4 but for January 15, 2017 (simulation of 2 days duration).

similar to the results from the summer nights (not shown). The sensitivity to *Pr* remains large, and there is an increase in sensitivity to α_5, which is only applied in stable conditions, likewise there is a large decrease in sensitivity to α_4 as it is only applied in unstable conditions. In addition, we expect the EDMF treatment to be less active in stable conditions and the reduced sensitivity to these parameters is found during the winter case. During the wintertime case there is also very little difference in the parameter sensitivity with day or night, which is consistent with persistent stable conditions over the diurnal cycle (not shown).

The differences seen in Figures 4 and 5 can be related to differences in wind speed in addition to differences in stability. The period around August 22 is marked by strong simulated winds ranging between 6.5 and 13 m s^{-1}, while the period on January 15 has much weaker simulated winds ranging between 2.8 and 7.3 m s^{-1}. Previous studies have shown how parameter sensitivities change with wind speed. To investigate the sensitivity to wind speed directly, the standardized range in wind speed caused by parameter perturbations is computed as a function of the domain average wind speed for the summer period (Figure 6). Similar results were found for the winter period (not shown). To compute the standardized range the results are divided into six discrete bins over the range of parameter values. The wind speed range is defined as the difference between the bins associated with the largest (bin 6) and smallest (bin 1) parameter values. This approach is similar to that used by Yang et al. (2017). The range of the domain average wind speed from each time (145 values in the 6 days simulation) are divided into 8 bins according to the ensemble mean wind speed. The mean range of the wind speed is standardized by dividing it by the mean ensemble standard deviation for each wind speed bin. The results show a large sensitivity to *Pr* for all wind speeds (Figure 6). Yang et al. (2017) showed strong sensitivity to *Pr* for both wind speeds less than 3 m s^{-1} and greater than 13 m s^{-1}, but found little sensitivity to *Pr* during unstable conditions, thus the large sensitivities seen in *Pr* here is likely due to increased sensitivity at night rather than the differences in wind speed in the two cases. Likewise, α_5 is only active in stable conditions and it is found to explain 2.9% of the total variance for the summer period (Figure 4) compared to 14.7% of the variance for the winter period with relatively weak winds (Figure 5). The standardized range of wind speed associated with α_5 is found to increase with wind speed (Figure 6e). Therefore, the increased sensitivity to α_5 in winter compared to summer is mainly due to more frequent stable conditions in winter, rather than the sensitivity to wind speed. The sensitivity to Z_f and *K* are found to be a function of the wind speed with larger values of wind speed leading to larger differences in the standardized range of wind speed but are largely independent of stability, consistent with the results of Yang et al. (2017).

There is a significant amount of spatial variability observed on August 22 and January 15, as shown in Figures 4 and 5. For example, during the daytime in the summer the amount of variance associated with *Pr* is

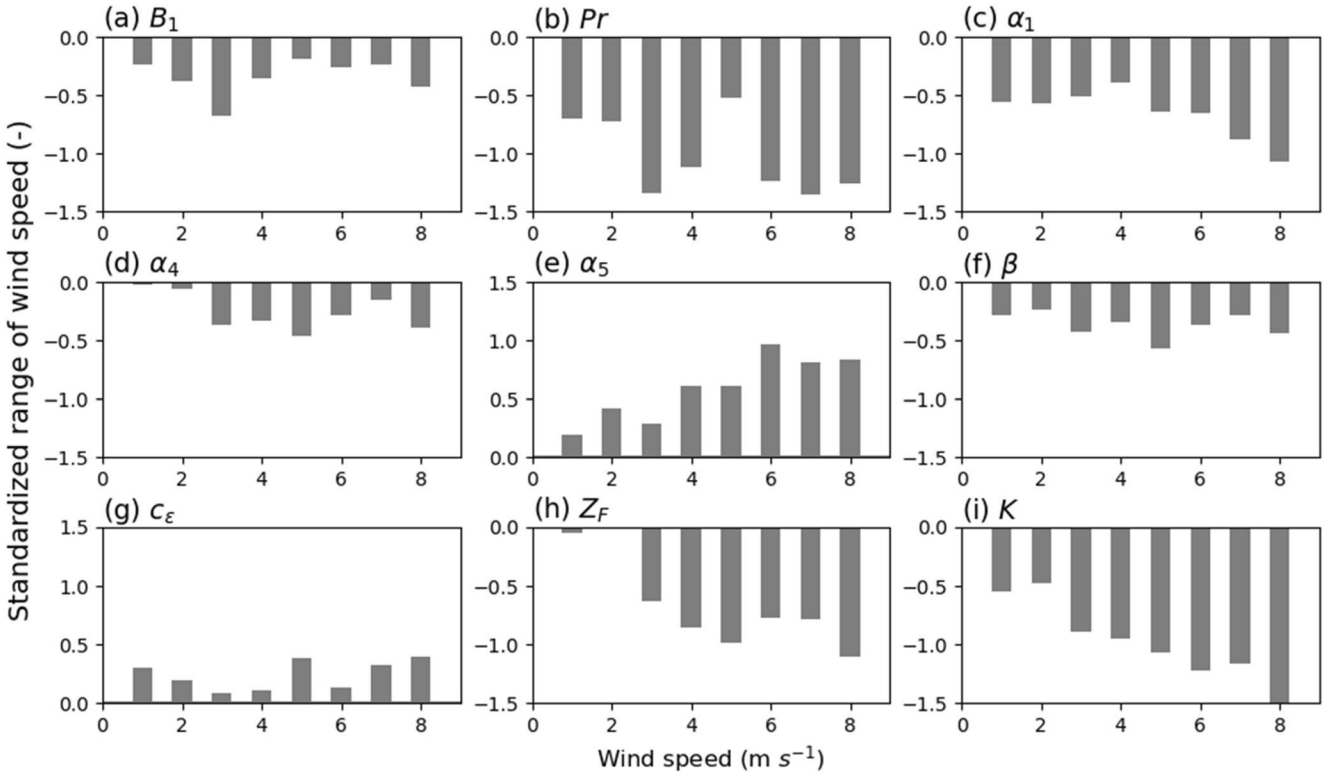

Figure 6. Response (bin 6 – bin 1 differences) of wind speed for the nine most influential parameters over different wind speed ranges for the summer case (August 18–24, 2016).

smaller over the Cascade Mountains and along the eastern edge of the Columbia Basin. The sensitivity to α_1 follows a different pattern with a relatively large impact over the higher elevations. At first glance these results seem to contradict the results of Yang et al. (2017), who showed little variability of the sensitivity to *Pr* and α_1 as function of terrain slope. It is important to note, however, that their results were computed from a month-long simulation while the results presented here are for a much shorter time period. Over the 6 days analysis period, the day-to-day variability in the sensitivity is large and the apparent dependence on the terrain elevation is much reduced if averaged over the period (not shown).

The results presented here show a much reduced sensitivity to B_1 than reported by Yang et al. (2017) and Berg et al. (2019). In this study, the range of B_1 was reduced to be 18–30 compared to the range of 12 and 36 used by Yang et al. (2017) and Berg et al. (2019), who selected the range to be ±50% from the default value in WRF. Other recent studies have used different ranges of B_1 and tended to look at smaller values of B_1, using ranges between 12 and 24 (Jahn et al., 2017; Muñoz-Esparza et al., 2018), or the default value of 24 used in WRF (Bodini et al., 2020). This change in the range of values in B_1 leads to a decreased sensitivity of the results to changes in B_1 compared to the earlier studies.

4.3. Change in Parameter Sensitivity as a Function of Simulation Duration

One goal of this study is to investigate the impact of parameter uncertainty as a function of simulation duration for conditions on August 22 and January 15. As shown in Figure 7, the mean simulated turbine-height wind speed on August 22 is nearly identical for simulation durations of 2 or 6 days (with domain means of 6.8 compared to 6.6 m s^{-1}), and very little pattern to the differences. Likewise, the standard deviation of turbine-height wind speed increases slightly for simulation durations of 2 and 6 days (0.3 compared to 0.2 m

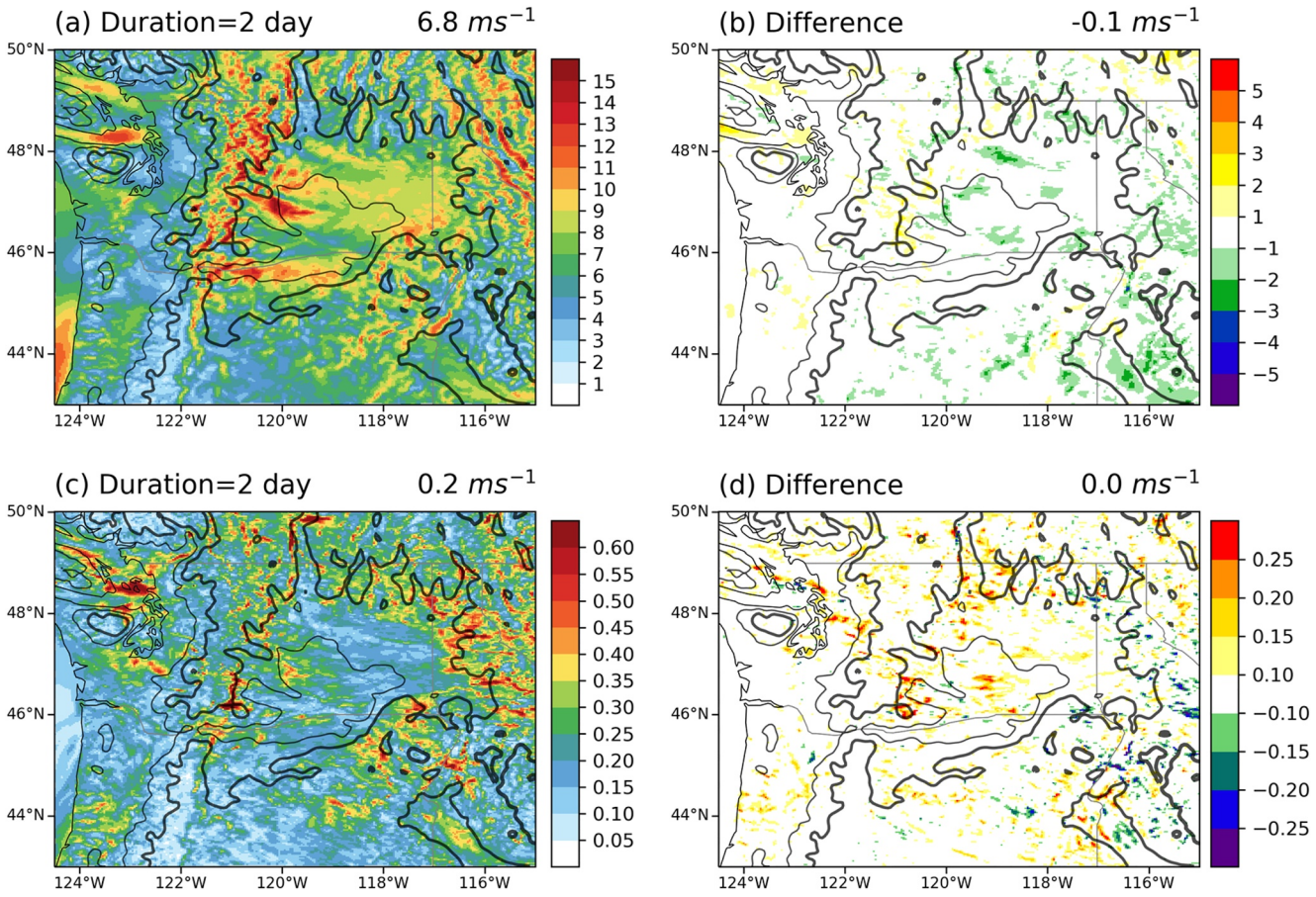

Figure 7. Daily mean wind speed (top) and inter-member standard deviation (bottom; colors) on August 22, 2016 for a simulation duration of 2 days (left) and the difference in wind speed for durations of 2 and 6 days (right). Lines indicate terrain elevations of 500 (thin) and 1,000 m (thick).

s^{-1} for a simulation duration of 2 days). The spatial pattern in the wind speed is also consistent across different days with relatively large wind speeds and standard deviations associated with topographic features and smaller wind speeds and standard deviations in many of the low-lying areas. There are some minor changes in the spatial distribution of the standard deviation, with larger values generally found in parts of the domain with higher elevation for a simulation duration of 6 days (Figure 7). The small changes in the standard deviation as a function of simulation duration is likely associated with the relatively small domain used in the study, meaning that the results are tightly constrained by the boundary conditions.

Similar to the results for summer, the mean and standard deviation does not change with simulation durations for January 15 (Figure 8). As is the case for summer, the largest mean values are generally associated with higher elevations, and relatively small values in the low-lying areas of the domain. For the winter cases, however, the sensitivity over the Cascade Mountains in the western part of the domain are more pronounced and can be explained in part by the need for longer simulations for the ensembles to become stable. In addition, much of the variability in the winter case can be associated with the value of *Pr* and α_5 (Figure 5). The sensitivity to *Pr*, which Yang et al. (2017) showed, increases some with terrain slope. Likewise, the results shown in Figure 5 show large values of α_5 in the same areas as the large amounts of variances shown in Figure 7d.

At first glance the tight constraint on the simulations might be construed as a weakness of the study, and indeed use of a larger domain could lead to a larger range in the PPE values. Alternatively, the study could have been constructed to more closely follow a forecasting procedure in which subsequent forecasts are started with initial and boundary conditions generated at later times. This approach, however, would convolute the relative impact of the initial and boundary conditions with the parameter uncertainty and make it more difficult to quantify the impact of the parameter uncertainty alone. In addition, Pichugina et al. (2019)

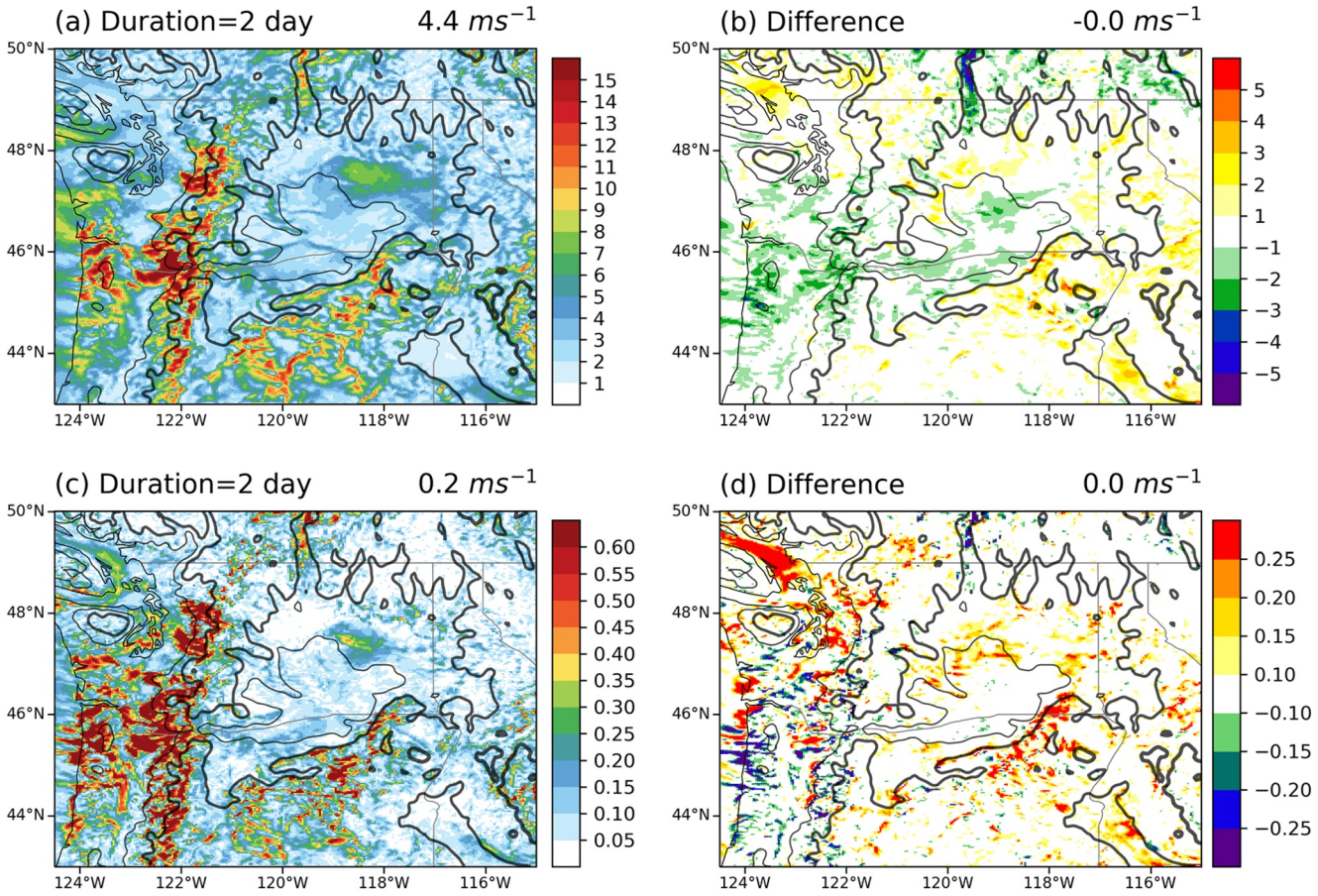

Figure 8. Same as Figure 7 but for January 15.

found that errors using the HRRR did not increase with time over the 15 h duration of the forecast, which they attributed to the strong influence of the topography in this area.

The negligible changes in standard deviations highlighted in Figures 7 and 8 is borne out in an analysis of the time series of averaged observed and simulated wind speed (Figures 2 and 3). In these figures, the width of the blue lines represents the range in the means from the various members of the PPE from the longest simulation period, and the width of the orange lines show range of means from the PPE for time series from progressively longer durations. In the summer case the orange lines overlap the blue lines after approximately the first 8–19 h of the simulation. In contrast to the summer, it takes approximately 17–24 h for the winter simulation curves to overlap. There are also additional periods, for example on January 14 and 15, in which the orange curve is noticeably below the blue curve, suggesting weaker constraints on the winter simulations.

4.4. Dependence on Diurnal Cycle

The previous section described the results as a function of simulation period and highlighted that the ensemble spread of the PPE stopped growing after a relatively short period. The simulation with 6 days durations in this study also provides an opportunity to examine the diurnal cycle of sensitivity to parameter values used in the MYNN-EDMF parameterization and how the sensitivity changes over the study period. As in Section 4.2, the generalized linear model (McCullagh & Nelder, 1989) was constructed using the simulation results to decompose the total variance of the WRF outputs (i.e., the turbine-height wind speed) into the contribution from different parameters.

Yang et al. (2017) and Berg et al. (2019) documented differences in parameterization sensitivity as a function of time of day, which corresponded to the application of different parameters in the boundary layer parameterization as a function of the atmospheric stability. Consistent results are found in this study. During the summer there is enhanced sensitivity to B_1, α_4, β, c_ε, and Z_F during the day (nominally 14:00–2:00 UTC) (Figure 9). In contrast to the summer, the winter period is marked by a weaker diurnal cycle that is similar to the nighttime summer results. There are only limited periods near solar noon during which the parameters associated with convective boundary layers are important, and it is clear the mass-flux component of the EDMF parameterization is rarely triggered so there is little sensitivity to those parameters during winter. It is also interesting to note that the interactions of the various parameters, as indicated by the white areas in Figure 9 is generally quite small, although the interaction also follows a diurnal cycle with larger values found during the day. There is also a large variance at the start of the winter study period, which is associated with a frontal passage through the study domain. During the summer the variance tends to be larger at night, which is partially associated with flow over and around the topography during stable conditions (not shown).

The results presented in Figure 9 show the dependence of the turbine-height wind speed on the various parameters. The sensitivity, however, is also found to vary with height (Figure 10) in ways that are consistent with Yang et al. (2017) and Berg et al. (2019). During the daytime, the sensitivity to *Pr*, c_ε, and Z_F decreases rapidly with height, while the sensitivity to B_1 and α_4 increases below approximately 300 m. Above that altitude, B_1 decreases and α_4 remains nearly constant. Results presented by Berg et al. (2019) also showed that the sensitivity to *Pr* tended to be larger when then sensitivity to B_1 is smaller. The sensitivity to β increases rapidly with height from the surface to approximately 600 m, and then increases more slowly. The increased sensitivity to α_4 and β with height is likely due to their impact on the length scales that change as function of altitude. The decrease in sensitivity to c_ε could be due to changes in difference between the ambient air and plume properties and changes in the updraft velocity with height.

The parameter sensitivity can also be examined as a function of normalized height (height above ground divided by the height of the convective boundary layer as determined in the MYNN-EDMF parameterization). This approach provides additional insight as the depth of the convective boundary layer changes throughout the day. The primary difference found viewing the results in this way, is a more constant dependence on B_1 over the depth of the convective boundary layer, increased sensitivity to *Pr* near the boundary layer top, and slightly larger sensitivity to the interactions between different parameters, particularly near the surface and at the top of the convective boundary layer. The sensitivities at night are also dependent on height, with

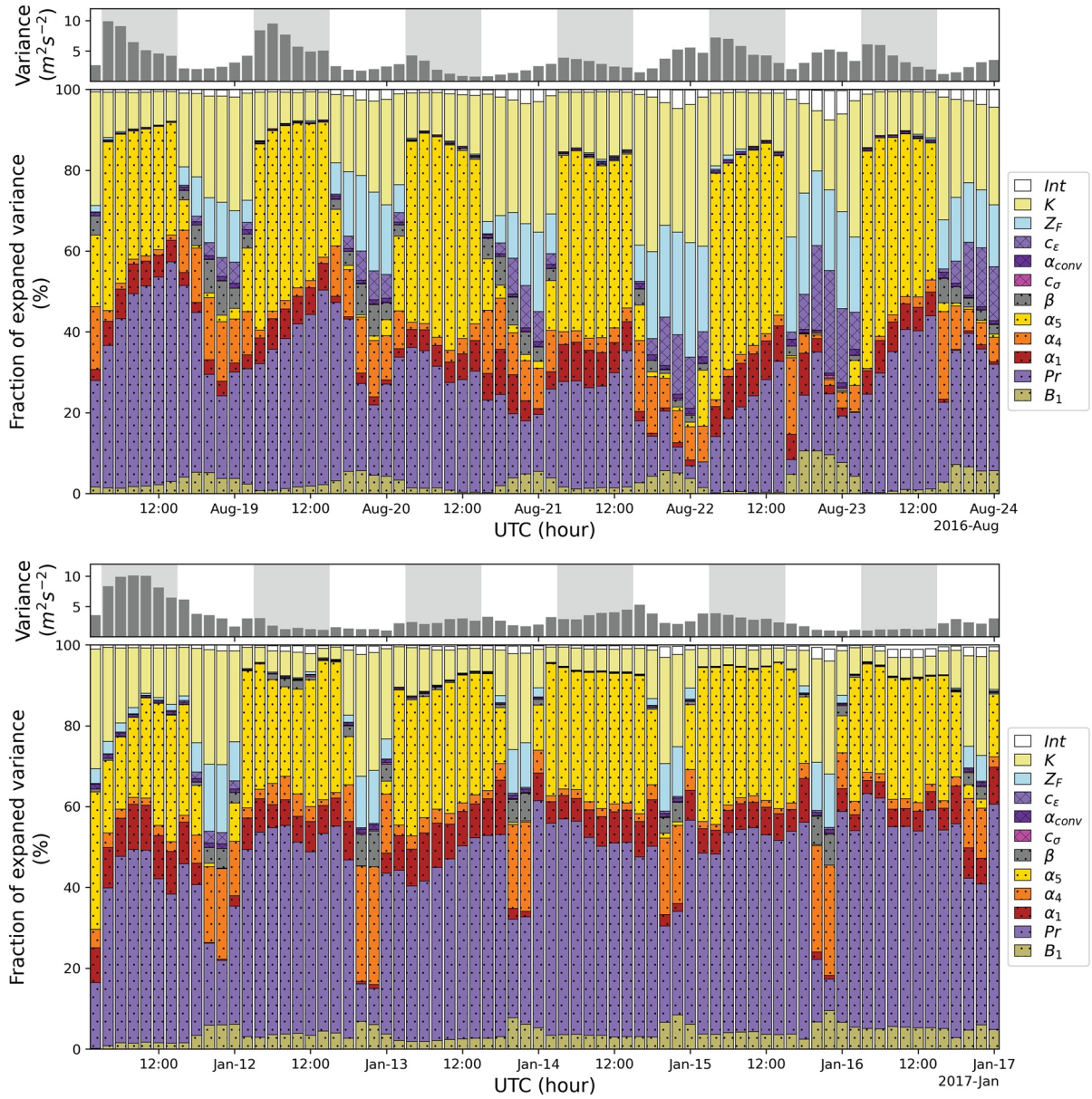

Figure 9. Fraction of the variance of turbine-height wind speed explained by each parameter as a function of time of day for each parameter during summer (top) and winter (bottom) for the simulation of 6 days duration across the entire simulation domain (colors). Int indicates the contribution of parameter interactions. Small panels indicate the total variance, as well as daytime (white) and nighttime (gray) conditions.

the sensitivity to *Pr* decreasing with height to an altitude of 400 m and then increasing for heights between 400 and 1,200 m, and decreasing sensitivity to α_5 with height. The decreases in the sensitivity with height is also consistent with the results presented by Yang et al. (2017). The nighttime sensitivity to c_ε is very small near the surface and slowly increases with height. The EDMF parameterization is generally inactive at night so the sensitivity is the result of periods earlier in the day when the EDMF parameterization was active.

The sensitivity to the parameters associated with the EDMF parameterization during the daytime increases through the six-day simulation period, as highlighted in Figure 9. Two reasons for the increased sensitivity is the steady increase in the fraction of the domain in which the mass-flux component of the parametrization is active (non-gray areas in Figure 11), and an increase in the EDMF updraft area (assumed to be the fraction of the grid box covered with convective updrafts determined in the parameterization) in the

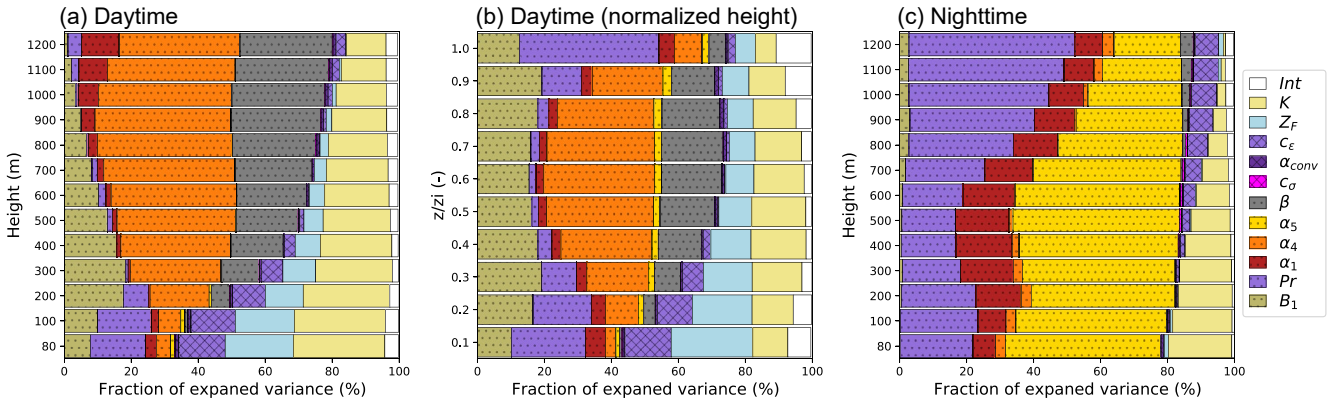

Figure 10. Fraction of variance explained by each parameter as a function of height (left and right panels) or normalized height (center) during daytime (left and center) and nighttime (right) during the summer for the simulation of 6 days duration across the entire simulation domain (colors).

WRF grid box during the simulation period (note that the maximum fractional area allowed in the EDMF is 10%). An alternate approach to examining the sensitivity to the EDMF parameters is to see how the parameter sensitivity changes as a function of EDMF updraft area (Figure 12). First, the values of modeled turbine-height wind speed were grouped according to the updraft area found over the time period 12:00–20:00 local time. Second, we applied a generalized linear model to calculate the variance contribution by different parameters for each bin. In this case, an EDMF updraft fractional area of 0 applies to grid columns were the mass-flux component of the EDMF parameterization is not active. When the convective plume representation is inactive and the MYNN-EDMF parameterization reverts back to the standard MYNN eddy-diffusivity mode, the results are most sensitive to K by a wide margin, followed by Z_F and Pr, which is consistent with results shown in Figure 2. As the updraft fraction increases, however, the sensitivity to K decreases significantly, sensitivity to Pr decreases slightly, while the sensitivity to Z_F and α_4 increases. The sensitivity to the surface roughness is due, at least in part, to the application of the Deardorff convective velocity scale in some of the EDMF calculations that maintains a sensitivity to the surface conditions. At

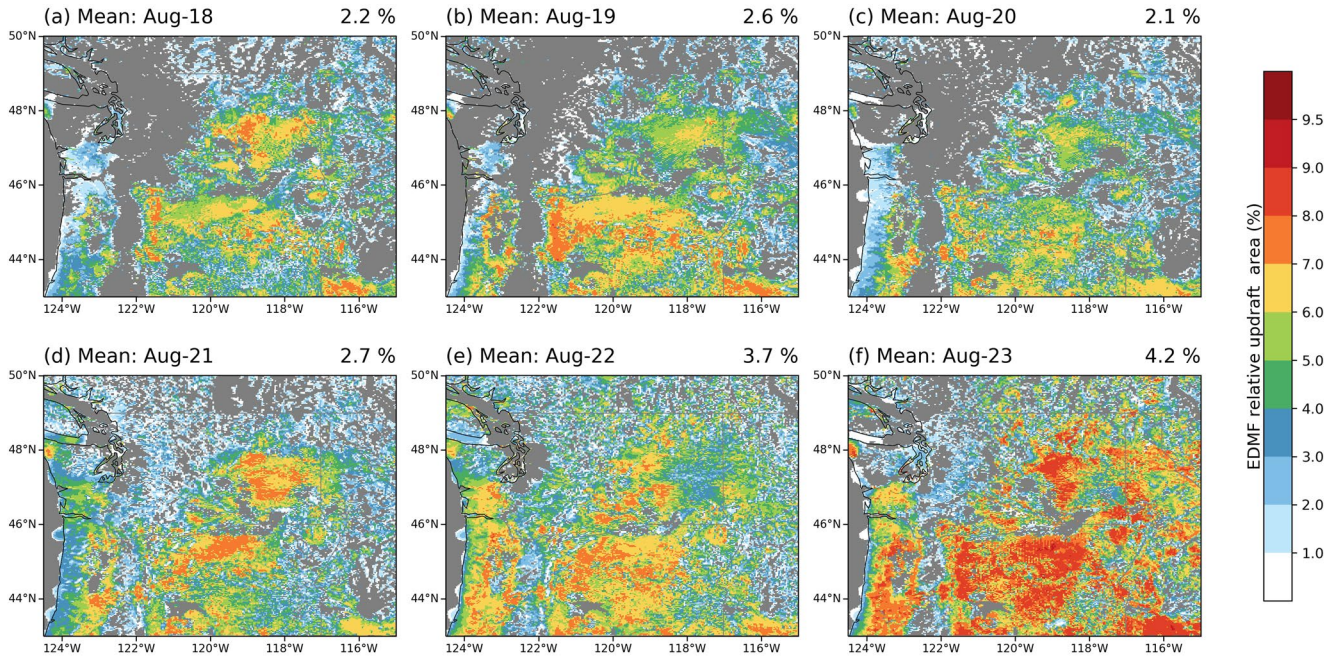

Figure 11. Updraft area computed from the EDMF part of the MYNN-EDMF parameterization for a simulation using the default parameter settings. Values are averaged from the surface to 1 km above ground and from 12:00 to 20:00 local time during the summer case study period. Gray indicates 0% updraft area.

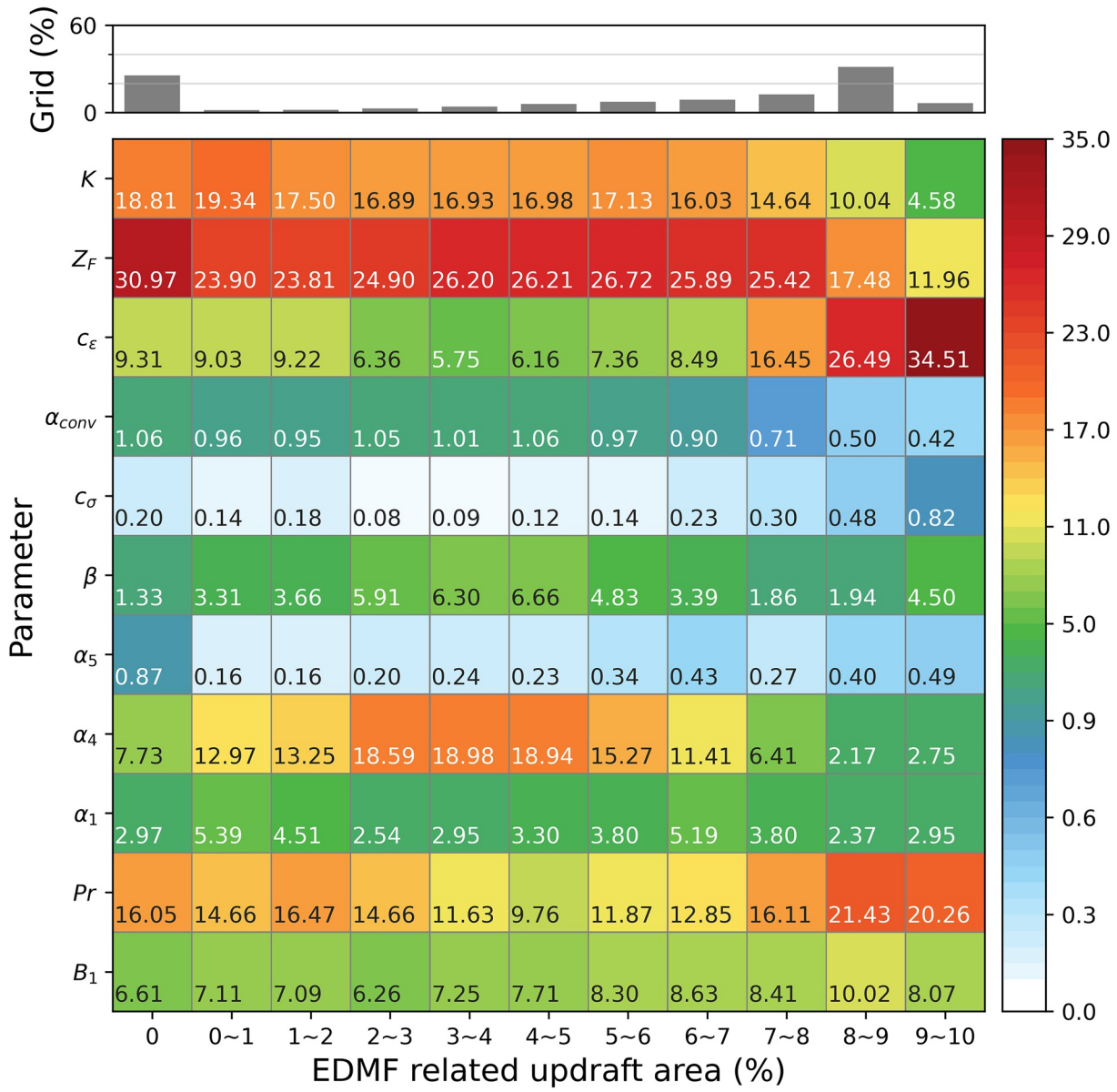

Figure 12. Fraction of the variance of turbine-height wind speed explained by each parameter (colors and numbers in boxes) as a function of EDMF updraft area on August 22, 2016. Box at the top shows the fraction of the domain with that EDMF updraft area.

large values of the updraft area (8%–10%) the sensitivity to c_ε increases significantly and becomes dominant. The sensitivity to c_ε when the updraft fraction is 0 is due to memory in the system from earlier time periods during which the mass-flux component was active.

5. Summary and Conclusions

This study investigates the sensitivity of wind speed, and particularly turbine-height wind speed, to the selection of parameter values in the MYNN-EDMF parameterization implemented in WRF by perturbing 11 parameters and constructing PPE for two different time periods, one in summer and one in winter, with relatively strong wind speeds during the summer and generally weaker winds in the winter. The parameters include those identified in earlier studies that contributed to the sensitivity in turbine-height wind speed for the standard MYNN parameterization as well as three parameters identified from the EDMF part of the

parameterization. In addition to the parameters identified in earlier studies that make large contributions to the sensitivity of the turbine-height wind speed, namely K, Z_F, Pr, and α_4, the results are found to be sensitive to the entrainment parameter, c_ε, during unstable conditions with large EMDF updraft fraction. The sensitivity to some parameters, α_5, Z_F, and K, were also found to increase with increasing wind speed. Not surprisingly, the PPE mean and standard deviation are insensitive to the EDMF parameters at night or during the winter, which is consistent with stable conditions. It is important to keep in mind, however, that the periods and simulations used in this analysis were generally cloud free so that sensitivity to the cloud parameters in the EDMF could be underestimated.

The PPEs were constructed to be of different durations, ranging from 2 to 6 days (all ending on the same day) to investigate how the parameter sensitivity changes with the duration. The parametric sensitivity is found to be insensitive to the length of the simulation after an initial period of 8–19 h in the summer and 17–24 h in the winter. This behavior suggests that the growth in the spread is associated with relatively fast processes in the model that are ultimately constrained by the boundary conditions and/or topography.

Analysis of the 6 days PPE allows the investigation of how the sensitivity to various parameters changes over the simulation period. These changes are associated with changes over the diurnal cycle and associated cycle of atmospheric stability, as well as systematic changes over the duration of the simulation. The sensitivity in the simulated turbine-height wind speed is found to change as a function of the convective updraft area in the mass-flux component of the EDMF scheme. During cases with large updraft areas the sensitivity to c_ε is larger than the sensitivity to any other parameters in the MYNN-EMDF parameterization. Similar to earlier analyses, the parameter sensitivity changes with the time of day as the stability changes. The sensitivity to c_ε suggests the need for additional research to more tightly constrain this parameter, or to determine if it should be a function of space and time rather than uniformly prescribed over the domain, which could have an impact on wind energy related forecasts.

The results presented in this study show the sensitivity of hub-height wind speed to a number of different model parameters. There are a number of important implications associated with this work. First, identification of parameters with the largest impact on the wind speed can be used to target future development of the MYNN-EDMF parameterization to those parts of the scheme that have the largest impact on the results, such as an improved representation of Pr. Second, the sensitivity to Z_F suggests the need for better estimates of the surface roughness that are truly representative of local conditions. Third, it provides guidance that can be applied in field studies to better constrain those parameters that have the largest impact on the results. For example, a field study or analysis of a wider range of large-eddy simulation could be conducted to better constrain α_4. Finally, the study highlights the temporal variability of the parametric uncertainty that can be used by those working to provide uncertainty estimates for day-ahead forecasts of the wind resource.

Acknowledgments
This work was supported by the Department of Energy's Wind Energy Technology Office. The authors thank the WFIP2 event loggers (Justin Sharp, Jaymes Kenyon, Bob Banta, Eric Grimit, Kyle Wade, Mark Stoelinga, Qing Yang, Eric James, Kyle Wade, Clara St. Martin) for their effort in cataloging events. The WFIP2 study was also made possible by a large number of individuals involved in the deployment of the sodars and Doppler lidars. The authors thank Colleen Kaul and Bob Banta for reviewing earlier versions of the manuscript. B. Y. thanks the support by the National Natural Science Foundation of China (41675101). Computational resources were provided by Wind Energy Technology Office and the National Renewable Energy Laboratory. PNNL is operated by DOE by the Battelle Memorial Institute under contract DE-A06-76RLO 1830.

Data Availability Statement

Data used in this manuscript are available from the Atmosphere to Electron Data Archive and Portal (https://a2e.energy.gov/about/dap).

References

Ancell, B. C. (2016). Improving high-impact forecasts through sensitivity-based ensemble subsets: Demonstration and initial tests. *Weather and Forecasting*, *31*(3), 1019–1036. https://doi.org/10.1175/waf-d-15-0121.1

Angevine, W. M. (2005). An integrated turbulence scheme for boundary layers with shallow cumulus applied to pollutant transport. *Journal of Applied Meteorology*, *44*(9), 1436–1452. https://doi.org/10.1175/jam2284.1

Angevine, W. M., Jiang, H., & Mauritsen, T. (2010). Performance of an Eddy Diffusivity-Mass Flux scheme for shallow cumulus boundary layers. *Monthly Weather Review*, *138*(7), 2895–2912. https://doi.org/10.1175/2010mwr3142.1

Banks, R. F., Tiana-Alsina, J., Baldasano, J. M., Rocadenbosch, F., Papayannis, A., Solomos, S., & Tzanis, C. G. (2016). Sensitivity of boundary layer variables to PBL schemes in the WRF model based on surface meteorological observations, lidar, and radiosondes during the HygrA-CD campaign, *Atmospheric Research*, *176–177*, 185–201. https://doi.org/10.1016/j.atmosres.2016.02.024

Banta, R. M., Pichugina, Y. L., Brewer, W. A., Choukulkar, A., Lantz, K. O., Olson, J. B., et al. (2020). Characterizing NWP model errors using Doppler-Lidar measurements of recurrent regional diurnal flows: Marine-air intrusions into the Columbia River Basin. *Monthly Weather Review*, *148*(3), 929–953. https://doi.org/10.1175/mwr-d-19-0188.1

Berg, L. K., Liu, Y., Yang, B., Qian, Y., Olson, J., Pekour, M., et al. (2019). Sensitivity of turbine-height wind speeds to parameters in the planetary boundary layer parametrization used in the weather research and forecasting model: Extension to wintertime conditions. *Boundary Layer Meteorology*, *170*(3), 507–518. https://doi.org/10.1007/s10546-018-0406-y

Bianco, L., Djalalova, I. V., Wilczak, J. M., Olson, J. B., Kenyon, J. S., Choukulkar, A., et al. (2019). Impact of model improvements on 80 m wind speeds during the second Wind Forecast Improvement Project (WFIP2). *Geoscientific Model Development*, *12*(11), 4803–4821. https://doi.org/10.5194/gmd-12-4803-2019

Bodini, N., Lundquist, J. K., & Optis, M. (2020). Can machine learning improve the model representation of TKE dissipation rate in the boundary layer for complex terrain? *Geoscientific Model Development Discussions*, *2020*, 1–21. https://doi.org/10.5194/gmd-2020-16

Caflisch, R. E. (1998). Monte Carlo and quasi-Monte Carlo methods. *Acta Numerica*, *7*, 1–49. https://doi.org/10.1017/S0962492900002804

Carvalho, D., Rocha, A., Gómez-Gesteira, M., & Santos, C. (2012). A sensitivity study of the WRF model in wind simulation for an area of high wind energy, *Environmental Modelling & Software*, *33*, 23–34. https://doi.org/10.1016/j.envsoft.2012.01.019

Chaboureau, J.-P., & Bechtold, P. (2002). A simple c parameterization derived from cloud resolving model data: Diagnostic and prognostic applications. *Journal of the Atmospheric Sciences*, *59*(15), 2362–2372. https://doi.org/10.1175/1520-0469(2002)059<2362:ascpdf>2.0.co;2

Chaboureau, J.-P., & Bechtold, P. (2005). Statistical representation of clouds in a regional model and the impact on the diurnal cycle of convection during Tropical Convection, Cirrus and Nitrogen Oxides (TROCCINOX). *Journal of Geophysical Research*, *110*(D17). https://doi.org/10.1029/2004JD005645

Constantinescu, E. M., Zavala, V. M., Rocklin, M., Lee, S., & Anitescu, M. (2011). A computational framework for uncertainty quantification and stochastic optimization in unit commitment with wind power generation. *IEEE Transactions on Power Systems*, *26*(1), 431–441. https://doi.org/10.1109/TPWRS.2010.2048133

Di, Z., Duan, Q., Gong, W., Wang, C., Gan, Y., Quan, J., et al. (2015). Assessing WRF model parameter sensitivity: A case study with 5 day summer precipitation forecasting in the Greater Beijing Area. *Geophysical Research Letters*, *42*(2), 579–587. https://doi.org/10.1002/2014gl061623

Dyer, A. J., & Hicks, B. B. (1970). Flux-gradient relationships in the constant flux layer. *Quarterly Journal of the Royal Meteorological Society*, *96*(410), 715–721. https://doi.org/10.1002/qj.49709641012

Etherton, B., & Santos, P. (2008). Sensitivity of WRF Forecasts for South Florida to Initial Conditions. *Weather and Forecasting*, *23*(4), 725–740. https://doi.org/10.1175/2007waf2006115.1

Fernández-González, S., Martín, M. L., García-Ortega, E., Merino, A., Lorenzana, J., Sánchez, J. L., et al. (2018). Sensitivity analysis of the WRF Model: Wind-resource assessment for complex terrain. *Journal of Applied Meteorology and Climatology*, *57*(3), 733–753. https://doi.org/10.1175/jamc-d-17-0121.1

Fernández-González, S., Martín, M. L., Merino, A., Sánchez, J. L., & Valero, F. (2017). Uncertainty quantification and predictability of wind speed over the Iberian Peninsula. *Journal of Geophysical Research: Atmospheres*, *122*(7), 3877–3890. https://doi.org/10.1002/2017jd026533

Iacono, M. J., Delamere, J. S., Mlawer, E. J., Shephard, M. W., Clough, S. A., & Collins, W. D. (2008). Radiative forcing by long-lived greenhouse gases: Calculations with the AER radiative transfer models. *Journal of Geophysical Research*, *113*(D13), D13103. https://doi.org/10.1029/2008jd009944

Jahn, D. E., Takle, E. S., & Gallus, W. A. (2017). Wind-ramp-forecast sensitivity to closure parameters in a boundary layer parametrization scheme. *Boundary Layer Meteorology*, *164*(3), 475–490. https://doi.org/10.1007/s10546-017-0250-5

Langhans, W., Mueller, J., & Collins, W. D. (2019). Optimization of the Eddy-Diffusivity/Mass-Flux shallow cumulus and boundary-layer parameterization using surrogate models. *Journal of Advances in Modeling Earth Systems*, *11*(2), 402–416. https://doi.org/10.1029/2018ms001449

Lu, W., & Zhong, S. (2014). A numerical study of a persistent cold air pool episode in the Salt Lake Valley, Utah. *Journal of Geophysical Research: Atmospheres*, *119*(4), 1733–1752. https://doi.org/10.1002/2013jd020410

McCaffrey, K., Wilczak, J. M., Bianco, L., Grimit, E., Sharp, J., Banta, R., et al. (2019). Identification and characterization of persistent cold pool events from temperature and wind profilers in the Columbia River Basin. *Journal of Applied Meteorology and Climatology*, *58*(12), 2533–2551. https://doi.org/10.1175/jamc-d-19-0046.1

McCullagh, P., & Nelder, J. A. (1989). *Generalized linear models* (Second ed.). Boca Raton, FL: Chapman and Hall/CRC.

Mesinger, F., DiMego, G., Kalnay, E., Mitchell, K., Shafran, P. C., Ebisuzaki, W., et al. (2006). North American regional reanalysis. *Bulletin of the American Meteorological Society*, *87*(3), 343–360. https://doi.org/10.1175/bams-87-3-343

Muñoz-Esparza, D., Sharman, R. D., & Lundquist, J. K. (2018). Turbulence dissipation rate in the atmospheric boundary layer: Observations and WRF mesoscale modeling during the XPIA field campaign. *Monthly Weather Review*, *146*(1), 351–371. https://doi.org/10.1175/mwr-d-17-0186.1

Nakanishi, M., & Niino, H. (2004). An improved Mellor-Yamada Level-3 model with condensation Physics: Its design and verification. *Boundary Layer Meteorology*, *112*(1), 1–31. https://doi.org/10.1023/b:boun.0000020164.04146.98

Nakanishi, M., & Niino, H. (2006). An improved Mellor-Yamada Level-3 Model: Its numerical stability and application to a regional prediction of advection fog. *Boundary Layer Meteorology*, *119*(2), 397–407. https://doi.org/10.1007/s10546-005-9030-8

Nakanishi, M., & Niino, H. (2009). Development of an improved turbulence closure model for the atmospheric boundary layer. *Journal of the Meteorological Society of Japan*, *87*(5), 895–912. https://doi.org/10.2151/jmsj.87.895

Nakanish, M. (2001). Improvement of the Mellor-Yamada turbulence closure model based on large-Eddy simulation data. *Boundary Layer Meteorology*, *99*(3), 349–378. https://doi.org/10.1023/a:1018915827400

Neggers, R. A. J. (2009). A dual mass flux framework for boundary layer convection. Part II: Clouds. *Journal of the Atmospheric Sciences*, *66*(6), 1489–1506. https://doi.org/10.1175/2008jas2636.1

Neggers, R. A. J., Köhler, M., & Beljaars, A. C. M. (2009). A dual mass flux framework for boundary layer convection. Part I: Transport. *Journal of the Atmospheric Sciences*, *66*(6), 1465–1487. https://doi.org/10.1175/2008jas2635.1

Nielsen-Gammon, J. W., Hu, X.-M., Zhang, F., & Pleim, J. E. (2010). Evaluation of planetary boundary layer scheme sensitivities for the purpose of parameter estimation. *Monthly Weather Review*, *138*(9), 3400–3417. https://doi.org/10.1175/2010mwr3292.1

Olson, J. B., Kenyon, J. S., Angevine, W. A., Brown, J. M., Pagowski, M., & Suselj, K. (2019). A description of the MYNN-EDMF scheme and the coupling to other components in WRF-ARW*Rep*. *NOAA Technical Memorandum OAR GSD-61*, NOAA.

Olson, J. B., Kenyon, J. S., Djalalova, I., Bianco, L., Turner, D. D., Pichugina, Y., et al. (2019). Improving wind energy forecasting through numerical weather prediction model development. *Bulletin of the American Meteorological Society*, *100*(11), 2201–2220. https://doi.org/10.1175/bams-d-18-0040.1

Pichugina, Y. L., Banta, R. M., Alan Brewer, W., Bianco, L., Draxl, C., Kenyon, J., et al. (2020). Evaluating the WFIP2 updates to the HRRR model using scanning Doppler lidar measurements in the complex terrain of the Columbia River Basin. *Journal of Renewable and Sustainable Energy*, *12*(4), 043301. https://doi.org/10.1063/5.0009138

Pichugina, Y. L., Banta, R. M., Bonin, T., Brewer, W. A., Choukulkar, A., McCarty, B. J., et al. (2019). Spatial variability of winds and HRRR-NCEP model error statistics at three Doppler-Lidar sites in the Wind-Energy generation region of the Columbia River Basin. *Journal of Applied Meteorology and Climatology*, *58*(8), 1633–1656. https://doi.org/10.1175/jamc-d-18-0244.1

Shaw, W. J., Berg, L. K., Cline, J., Draxl, C., Djalalova, I., Grimit, E. P., et al. (2019). The Second Wind Forecast Improvement Project (WFIP2): General Overview. *Bulletin of the American Meteorological Society*, *100*(9), 1687–1699. https://doi.org/10.1175/bams-d-18-0036.1

Shi, Y., Davis, K. J., Zhang, F., & Duffy, C. J. (2014). Evaluation of the parameter sensitivities of a coupled land surface hydrologic model at a critical zone observatory. *Journal of Hydrometeorology*, *15*(1), 279–299. https://doi.org/10.1175/jhm-d-12-0177.1

Siebesma, A. P., Soares, P. M. M., & Teixeira, J. (2007). A combined Eddy-Diffusivity Mass-Flux approach for the convective boundary layer. *Journal of the Atmospheric Sciences*, *64*(4), 1230–1248. https://doi.org/10.1175/jas3888.1

Skamarock, W. C., Klemp, J. B., Dudhia, J., Gill, D. O., Barker, D. M., Duda, M. G., et al. (2008). A description of the advanced research WRF version. *3Rep. NCAR/TN-475+STR, NCAR*.

Smirnova, T. G., Brown, J. M., & Benjamin, S. G. (1997). Performance of different soil model configurations in simulating ground surface temperature and surface fluxes. *Monthly Weather Review*, *125*(8), 1870–1884. https://doi.org/10.1175/1520-0493(1997)12510.1175/1520-0493(1997)125<1870:podsmc>2.0.co;2

Smirnova, T. G., Brown, J. M., Benjamin, S. G., & Kenyon, J. S. (2016). Modifications to the Rapid Update Cycle Land Surface Model (RUC LSM) available in the Weather Research and Forecasting (WRF) Model. *Monthly Weather Review*, *144*(5), 1851–1865. https://doi.org/10.1175/mwr-d-15-0198.1

Smirnova, T. G., Brown, J. M., Benjamin, S. G., & Kim, D. (2000). Parameterization of cold-season processes in the MAPS land-surface scheme. *Journal of Geophysical Research*, *105*(D3), 4077–4086. https://doi.org/10.1029/1999jd901047

Smith, N. H., & Ancell, B. C. (2019). Variations in parametric sensitivity for wind ramp events in the Columbia River Basin. *Monthly Weather Review*, *147*(12), 4633–4651. https://doi.org/10.1175/mwr-d-19-0019.1

Soares, P. M. M., Miranda, P. M. A., Siebesma, A. P., & Teixeira, J. (2004). An eddy-diffusivity/mass-flux parametrization for dry and shallow cumulus convection. *Quarterly Journal of the Royal Meteorological Society*, *130*(604), 3365–3383. https://doi.org/10.1256/qj.03.223

Sommeria, G., & Deardorff, J. W. (1977). Subgrid-scale condensation in models of nonprecipitating clouds. *Journal of the Atmospheric Sciences*, *34*(2), 344–355. https://doi.org/10.1175/1520-0469(1977)03410.1175/1520-0469(1977)034<0344:sscimo>2.0.co;2

Suselj, K., Posselt, D., Smalley, M., Lebsock, M. D., & Teixeira, J. (2020). A new methodology for observation-based parameterization development. *Monthly Weather Review*, *148*, 4159–4184. https://doi.org/10.1175/mwr-d-20-0114.1

Sušelj, K., Teixeira, J., & Matheou, G. (2012). Eddy diffusivity/mass flux and shallow Cumulus boundary layer: An updraft PDF multiple mass flux scheme. *Journal of the Atmospheric Sciences*, *69*(5), 1513–1533. https://doi.org/10.1175/jas-d-11-090.1

Tan, Z., Kaul, C. M., Pressel, K. G., Cohen, Y., Schneider, T., & Teixeira, J. (2018). An extended Eddy-diffusivity mass-flux scheme for unified representation of subgrid-scale turbulence and convection. *Journal of Advances in Modeling Earth Systems*, *10*(3), 770–800. https://doi.org/10.1002/2017ms001162

Thompson, G., & Eidhammer, T. (2014). A study of aerosol impacts on clouds and precipitation development in a large winter cyclone. *Journal of the Atmospheric Sciences*, *71*(10), 3636–3658. https://doi.org/10.1175/jas-d-13-0305.1

Thompson, G., Field, P. R., Rasmussen, R. M., & Hall, W. D. (2008). Explicit forecasts of winter precipitation using an improved bulk microphysics scheme. Part II: Implementation of a new snow parameterization. *Monthly Weather Review*, *136*(12), 5095–5115. https://doi.org/10.1175/2008mwr2387.1

Tian, Y., & Kuang, Z. (2016). Dependence of entrainment in shallow cumulus convection on vertical velocity and distance to cloud edge. *Geophysical Research Letters*, *43*(8), 4056–4065. https://doi.org/10.1002/2016gl069005

Wilczak, J. M., Stoelinga, M., Berg, L. K., Sharp, J., Draxl, C., McCaffrey, K., et al. (2019). The Second Wind Forecast Improvement Project (WFIP2): Observational Field Campaign. *Bulletin of the American Meteorological Society*, *100*(9), 1701–1723. https://doi.org/10.1175/bams-d-18-0035.1

Wilson, T. H., & Fovell, R. G. (2016). Modeling the Evolution and Life Cycle of Stable Cold Pools. *Weather and Forecasting*, *31*(6), 1753–1769. https://doi.org/10.1175/waf-d-16-0108.1

Xu, Z., Chen, J., Jin, Z., Li, H., & Chen, F. (2020). Assessment of the forecast skill of multiphysics and multistochastic methods within the GRAPES regional ensemble prediction system in the East Asian Monsoon Region. *Weather and Forecasting*, *35*(3), 1145–1171. https://doi.org/10.1175/waf-d-19-0021.1

Yang, B., Berg, L. K., Qian, Y., Wang, C., Hou, Z., Liu, Y., et al. (2019). Parametric and structural sensitivities of turbine-height wind speeds in the boundary layer parameterizations in the weather research and forecasting model. *Journal of Geophysical Research: Atmospheres*, *124*(12), 5951–5969. https://doi.org/10.1029/2018jd029691

Yang, B., Qian, Y., Berg, L. K., Ma, P.-L., Wharton, S., Bulaevskaya, V., et al. (2017). Sensitivity of turbine-height wind speeds to parameters in planetary boundary layer and surface-layer schemes in the weather research and forecasting model. *Boundary Layer Meteorology*, *162*(1), 117–142. https://doi.org/10.1007/s10546-016-0185-2

Zhong, S., Whiteman, C. D., Bian, X., Shaw, W. J., & Hubbe, J. M. (2001). Meteorological processes affecting the evolution of a wintertime cold air pool in the Columbia Basin. *Monthly Weather Review*, *129*(10), 2600–2613. https://doi.org/10.1175/1520-0493(2001)12910.1175/1520-0493(2001)129<2600:mpateo>2.0.co;2